Three-dimensional simulation of cavitating flow in real journal bearing geometry

Marcus SCHMIDT [1,*], Peter REINKE [1], Matthias NOBIS [1], Marco RIEDEL [1]

* Corresponding author: Tel.: ++49 (0)375 536 3893; Fax: ++49 (0)375 536 3393; Email: marcus.schmidt@fh-zwickau.de
[1] Institut für Kraftfahrzeugtechnik, Westsächsische Hochschule Zwickau, GERMANY

Abstract Hydrodynamic journal bearings are commonly used in many technical applications because they provide low friction and minimal wear. In general, flow simulation during the engineering design process is carried out by means of the Reynolds equation. The Reynolds equation is a non-linear two-dimensional differential equation, which is based on the pressure and the gap between shaft and bushing in relation to bearing clearance, eccentricity, bushing deformation and load. However, due its two-dimensional nature it is inaccurate where the lubricant flow inside the bearing becomes three-dimensional e.g., in the vicinity of feed holes or grooves. The work on hand presents the numerical approach and the cavitation model based on the Rayleigh-Plesset equation. Moreover, a bearing flow experiment was designed and constructed with the goal to validate numerical results. Finally, the validated 3D simulation model is applied on a real bearing, which was subject to an experimental investigation targeting cavitation. The numerical results include images of complex three-dimensional flow structures, vortices and vapor distributions. In comparison of 2D and 3D simulation, the two-dimensional approach gives wrong information in 2 out of 6 critical regions pertaining cavitation failing in both, over- and under-prediction of cavitation. In summary, a new numerical model expands the scope for the numerical simulation of the lubricant flow in hydrodynamic journal bearings and improves the prediction of cavitation.

Keywords: Micro Flow, Journal Bearing, Cavitation, CFD

1. Introduction

Hydrodynamic journal bearings are widely used in technical and industrial applications due to their favorable wearing quality and operating characteristics. In general, flow simulation during the engineering design process is carried out by means of the Reynolds equation which is a non-linear two-dimensional differential equation. Due its two-dimensional nature it is inaccurate where the lubricant flow inside the bearing becomes three-dimensional e.g., in the vicinity of feed holes or grooves shown in previous works [1] and [2]. Moreover, in flow regions where the pressure drops locally below the vapor pressure of the lubricant gas bubbles are generated which in turn change the flow field forming three-dimensional structures. Under certain conditions, when the bubbles implode adjacent to the bushing cavitation damage is produced and leads to erosion of bearing material up to the breakdown of the bearing system. To understand those mechanisms, which lead to local cavitation damages in hydrodynamic journal bearings, it is necessary to understand the three-dimensional nature of the lubricating flow inside the bearing. These complex and fully three-dimensional 2-phase flows can only be described with appropriate numerical models based on the Navier-Stokes equations including a cavitation model referring to Sauer [3]. A flow experiment was designed based on geometrical parameters transferred from a real bearing [4] to the test rig at a scale of 3:1. Reynolds and mechanical similarity rules are observed. The scaled experiment allows measurements of velocity profiles inside the fluid film across the gap between rotor and housing by means of Laser Doppler Velocimetry (LDV). To validate the phase change model in similar geometry to journal bearing, experimental data from Jakobsson/Floberg [5] are used and compared

to other numerical work done by Cullipard et al.[6]. This paper presents numerical results, include images of complex three-dimensional flow structures, vortices and vapour distributions inside the lubricant gap. The Results are compared with experimental data and conventional 2D-calculations regarding to critical cavitation zones in the journal bearing.

2. Approach

2.1 Geometrical parameters

A bearing system can be simplified by a fixed outer cylinder and a rotating inner cylinder. The eccentricity is given by the displacement e between both cylinder centre axes. In the outer cylinder, at half of breadth B is a feedhole for supplying the system with fresh fluid. The inner cylinder includes the exit holes, through which the fluid leaves the system. The Figure 1 shows the accordingly geometrical setup.

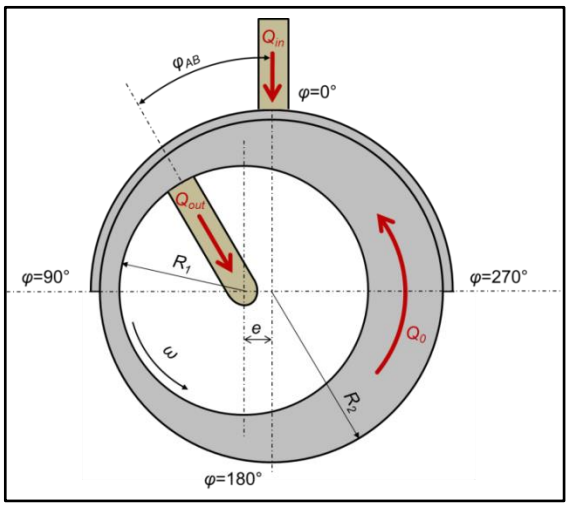

Fig. 1: Geometrical parameters of the bearing model

The basic parameters are

$$H_0 = R_2 - R_1 \quad (1) \qquad \Psi = \frac{H_0}{R_1} \quad (2)$$

$$U_1 = \omega \cdot R_1 \quad (3) \qquad \mathrm{Re} = \frac{H_0 \cdot U_1}{\upsilon} \quad (4)$$

$$\varepsilon = \frac{e}{H_0} \quad (5) \qquad Q_0 = 0{,}5 \cdot B \cdot H_0 \cdot U_1 \quad (6)$$

including the clearance H_0, the normalized clearance Ψ, the circumferential velocity U_1, the Reynolds number Re, the relative eccentricity ε and the main volume flow Q_0. Where index *1* indicates the rotating inner cylinder or the shaft and index *2* marks the outer cylinder or the bushing. General constants are indexed with *0*.

2.2 Numerical setup

The numerical simulations were performed using the software OpenFOAM. The code is based on the finite volume method and uses the three-dimensional, incompressible Navier-Stokes-Equations (eq.7) and the mass balance equation (eq.8).

$$\frac{\partial \rho \mathbf{u}}{\partial t} + \rho(\mathbf{u} \cdot \nabla)\mathbf{u} = \rho \cdot g - \nabla p + \mu \nabla^2 \mathbf{u} \quad (7)$$

$$\frac{\partial \rho}{\partial t} + \nabla \cdot (\rho \mathbf{u}) = 0 \quad (8)$$

To consider a second phase and the phase change an expanded transport equation (eq.9) has to be solved.

$$\frac{\partial \alpha}{\partial t} + \nabla \cdot (\alpha\, \mathbf{u}) + \nabla \cdot [\alpha(1-\alpha)u_\alpha] = \frac{\dot{m}^+ + \dot{m}^-}{\rho_l} \quad (9)$$

The volume fraction α depends on the volume of liquid V_l and the volume of vapour V_v in a cell and is calculated with eq. 10.

$$\alpha = \frac{V_l}{V_l + V_v} \quad (10)$$

The third term in eq. 9 is only significant at the interface between the liquid and vapour phase. If α = 1 (liquid, index *l*) or α = 0 (vapour, index *v*) the term disappears. The velocity of the compression from the interface is given by the value u_α. The source term on the right side of eq. 9 describes vaporisation $\dot{m}^+$ and condensation $\dot{m}^-$. For this source term a bubble dynamic approach according to Sauer [3] is used.

The transfered mass is calculated by eq. 11.

$$\dot{m} = \frac{\rho_l \rho_v}{\rho} \frac{3\alpha_{Nuc}}{R} (1 - \alpha_{Nuc}) \cdot \; sign[p_v - p] \cdot \dot{R} \cdot \begin{cases} C_C \; if \; sign[p_v - p] = -1 \\ C_V \; if \; sign[p_v - p] = 1 \end{cases} \quad (11)$$

The density ρ and the viscosity v are calculated as a mixture depends on α.

$$\rho = \rho_l \alpha \; + \rho_v \, (1 - \alpha) \quad (12)$$

$$v = v_l \, \alpha + v_v \, (1 - \alpha) \quad (13)$$

The ratio of vapour α_{Nuc} depends on the radius of the nuclei R and the number of nuclei n_0 per cubic meter.

$$\alpha_{Nuc} = \frac{\frac{4}{3}\pi R^3 n_0}{1 + \frac{4}{3}\pi R^3 n_0} \quad (14)$$

The bubble dynamic approach included by the simplified Rayleigh-Plesset equation 15 to determine the velocity of the nuclei wall.

$$\dot{R} = \sqrt{\frac{2}{3} \cdot \frac{|p_v - p|}{\rho_l}} \quad (15)$$

To adapt the solver for special cases two dimensionless constants C_C and C_V are used. They have a linear influence on the transfered mass of vapour or liquid. In the vicinity of the interface between vapour and liquid eq. 7 is extended by the surface tension σ. Therefore, the momentum equation is given by:

$$\frac{\partial \rho \mathbf{u}}{\partial t} + \rho(\mathbf{u} \cdot \nabla)\mathbf{u} = \rho \cdot g - \sigma \frac{1}{R}\mathbf{n} - \nabla p + \mu \nabla^2 \mathbf{u} \quad (16)$$

In Fig. 2 the volume mesh of the bearing model is shown. The model is built by a block-structured mesh with nearly orthogonal cells in the gap.

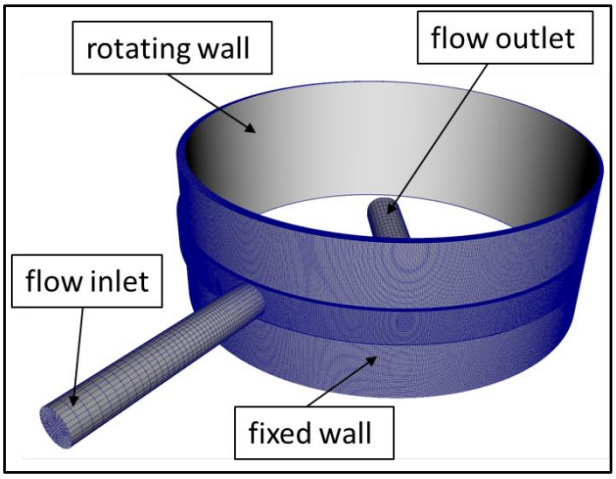

Fig. 2: Meshed simulation model

With this meshing method every cell has a unique relationship to the next cell neighbor and increases consequently the efficiency of the numerical solver. The necessary numerical discretization of 14 radial cells in the gap guarantees a sufficient numerical accuracy which was confirmed in previous work [2]. The overall solution domain consists of 2.2 million cells.
For the feed hole as well as the outlet hole a typical O-grid with wall adapted cells is used.
The position of the boundary condition at the inlet of the feedhole is modeled far away from the main solution domain to eliminate the influence of the boundary condition

2.3 Experimental setup

The experimental test rig (Fig.3) at a scale of 3:1 consists of a stationary outer cylinder and the rotating inner cylinder. For a free optical access the two cylinders are made of acrylic glass.
A significant difference between the test rig and a real journal bearing is the relative gap width. The test rig has a relative gap width of $\psi \approx 2.5$ %. However, a real journal bearing has a relative gap width near $\psi \approx 0.1$ %.

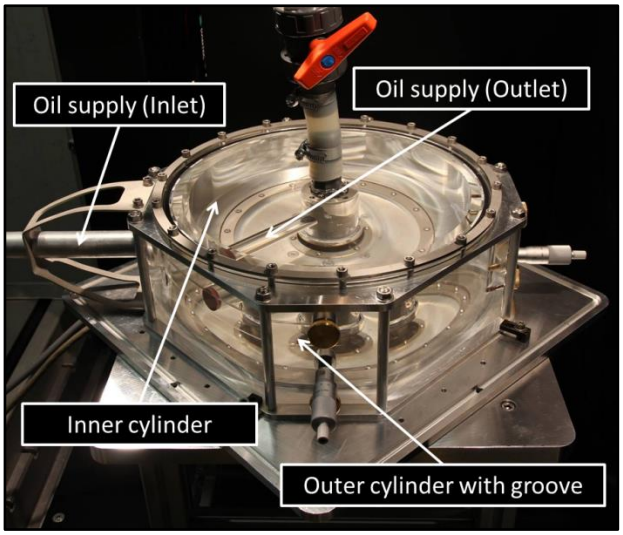

Fig. 3: Experimental test rig

Increasing the gap width at the test rig is absolutely necessary in order to provide a sufficient optical access to the LDV. Moreover, by choosing silicon oil with an appropriate viscosity and an adjusted circumferential speed of the inner cylinder Reynolds and mechanical similarity rules are observed.

The outer cylinder is positioned in an eccentric position with respect to the inner cylinder. Positioning of the LDV is achieved by rotating the assembly to the desired angular position and displacing the LDV-optic radially and vertically.

2.3 Validation of the flow model

The fluid flow is validated by comparing the measured circumferential velocity across the gap with the simulation point data. Figure 4 shows a comparison of selected experimental and numerical velocity profiles under the given setting parameters in a scaled diagram.
The numerical simulation is in perfect agreement with the experimental measurement. The normalized velocity u/U_1 is exactly one at the surface of the inner cylinder ($y/h = 0$). Accordingly, the normalized velocity is zero at the surface of the stationary outer cylinder ($y/h = 1$). A typical area of reversed flow is found adjacent to the outer cylinder and inside the groove.

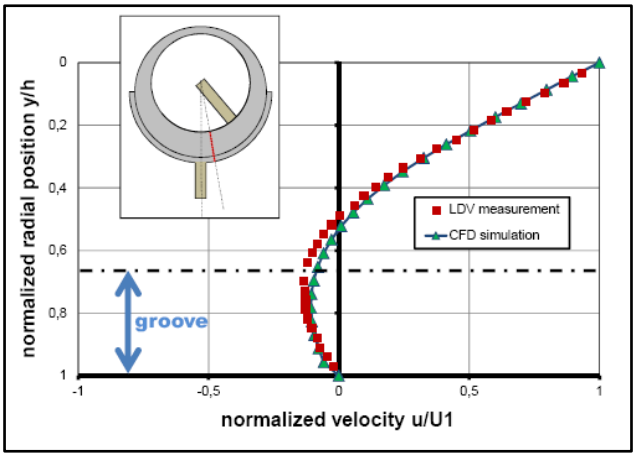

Fig. 4: Velocity profiles of a LDV and CFD at $\varphi = 8{,}96°$ for $\psi = 2{,}5\%$, $Re = 35$, $\varepsilon = 80\%$, $\varphi_{AB} = 40°$

2.4 Validation of the 2-phase model

The 2-phase flow and the phase change model was compared with J/F results [5].
The J/F experiment consists of a simple eccentric arrangement of a fixed outer bushing and rotating shaft similar to a bearing system without any supply flow. The fluid between the cylinder is oil with an vapour pressure of 20 kPa.

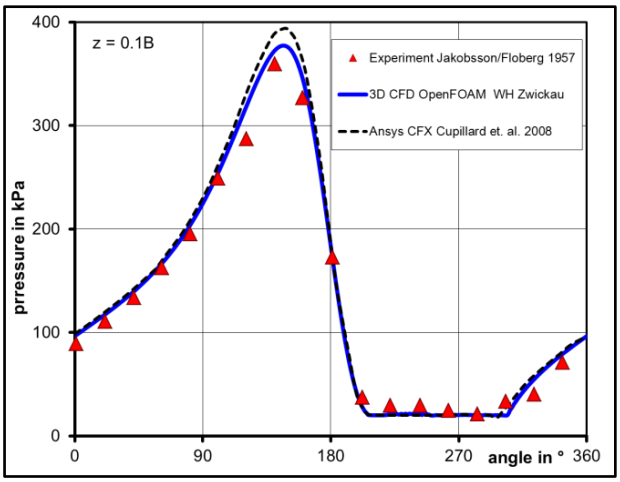

Fig. 5: Circumferential pressure plot of CFD and Experiment [4]

Figure 5 presents the comparison of the pressure distribution over the circumference from CFD done by the presented OpenFOAM-Code (blue line) to the experimental data. The simulation fits the experimental points regarding to the maximum pressure peak upstream of the minimum gap and the vapour region in the divergent gap. The vapour region is characterized by an isobaric pressure profile.

For further references, the Ansys CFX calculation done by Cullipard [6] with identically setup parameters.

3 Results

The power of the word on hand is demonstrated when the 3D-CFD code including 2-phase model is applied to experiment carried out by Wollfarth [4]. Figure 6 illustrates the cavitation investigation of the Experiment compared to the simulation with the basic 2D-Reynolds equation done in [7]. Wollfarth found two forms of cavitation: flow introduced cavitation marked with green rectangle and impact cavitation marked with orange rectangle. Taking the experimental parameters and setting the cavitation behavior was computed a) with a state-of-the-art 2D Modell and b) under the newly developed 3D-CFD code including 2-phase model.

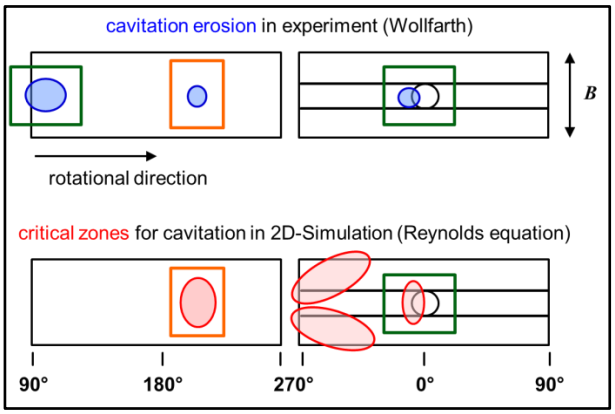

Fig. 6: Cavitation experiment and 2D-Simulation

The 2D simulation carried out two critical regions which are as well predicted in experiment. The critical areas are in the divergent gap at an angle of 200° and upstream in the vicinity of the inlet feedhole. An over prediction is found at the beginning of the groove at 270°, were the experiment shows no cavitation erosion. Additionally, cavitation damage is found in the experiment at the end of the groove at an angle of 90°, which is not predicted by the 2D simulation.
Therefore, a detailed 3D simulation is needed to capture three-dimensional flow structures and the behavior of vapour fraction in critical areas.

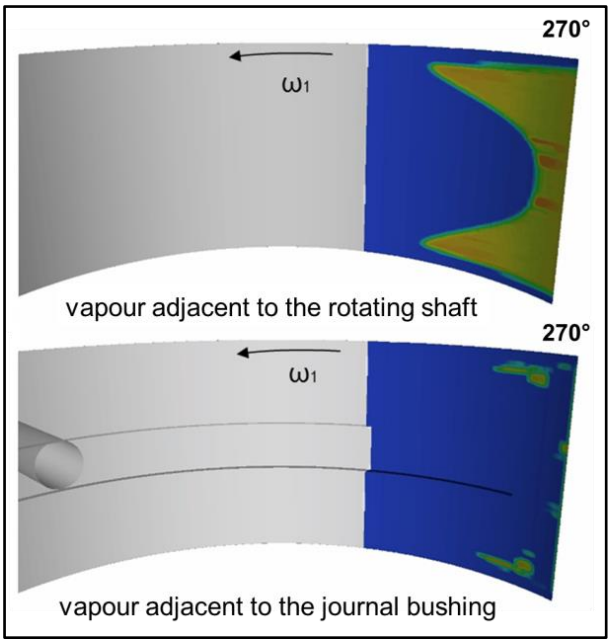

Fig. 7: 3D-CFD vapour fraction in real journal bearing in the divergent gap

The distribution of the vapour fraction in the divergent gap at an angle of 270° is shown in Fig. 7. The upper picture illustrates the vapour close to the surface of the rotating shaft and the lower picture the distribution on the bushing. The vapour transported close to the shaft above and below the groove in rotational direction. The vapour stratifies from the shaft to the fixed bushing in the radial gap. Hence, the two-dimensional calculation must fail in capturing the radial distribution. Furthermore, the experiment showed no cavitation due to low vapour fraction close to the bushing.

The Fig. 9 presents a comparison of 3D-Simulation to a photo of the bushing with cavitation damages from experiment. The vapour fraction distribution at the end of the groove from 3D-Simulation is similar size and in the same local position to the experimental erosion pattern. The flow at the end of the groove in rotational direction is similar to a forward face step flow. By overflowing the sharp edge a strong three-dimensional flow structure behind and along the grooves edges is generated. In addition with a reduction of the flow cross section, the flow accelerates and the hydrodynamic pressure drops below the vapour pressure of the fluid.

A vapour zone above the bushing is the result.

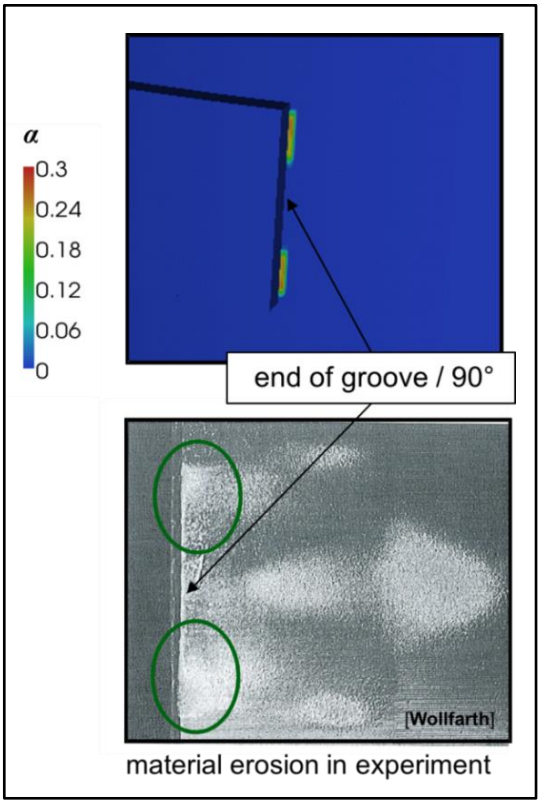

Fig. 9: 3D-CFD vapour fraction in real journal bearing at the end of groove

A critical cavitation area with a experimental damage is found upstream of the inlet feedhole. The vapour is created when the outlet feedhole is approaching the inlet feed hole. The amount of incoming oil flows directly to the outlet. The pressure in the vicinity of the feedhole reduces by high velocity flow around the feedhole edges.

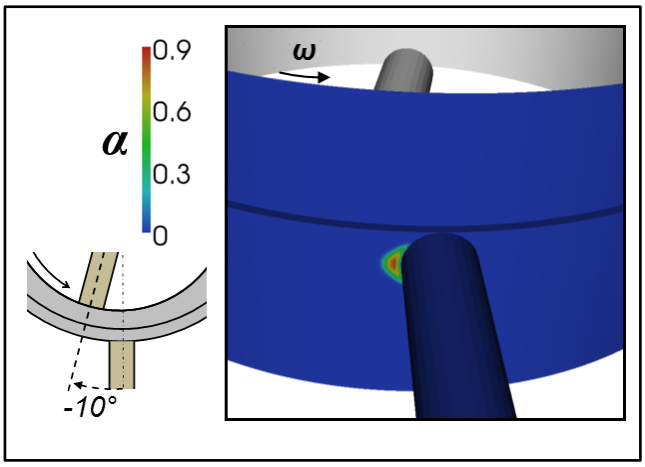

Fig. 8: 3D-CFD vapour fraction in real journal bearing in the vicinity of the inlet feedhole

A detail picture of vapour bubble fraction inside of the outlet feedhole is shown in Fig. 10. This vapour distribution is caused by inertia of the fluid. There is a large fluid flow through the outlet, when the outlet feedhole moves along the groove. Finally, the exit hole overlaps the end of the groove and the fluid flow is cut off. Hence, the pressure inside the feedhole decreases due fluid inertia.

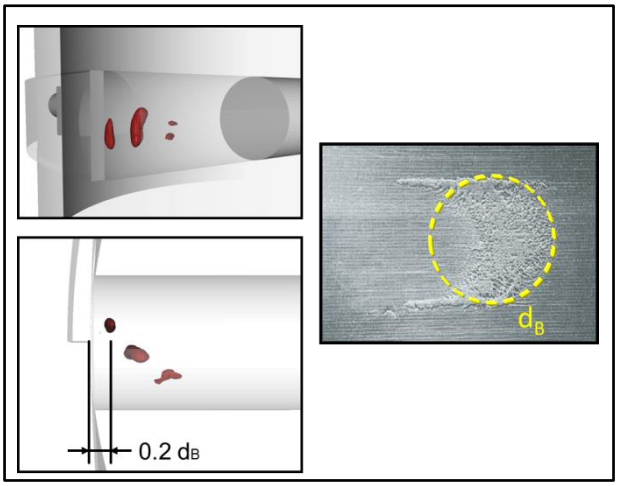

Fig. 10: 3D-CFD vapour fraction in real journal bearing in the outlet feedhole

Formed vapour bubbles remain inside the rotating feedhole and are transported in rotational direction towards the region with the minimum gap, where the shaft is close to the bushing wall. Under certain conditions, when the bubbles implode adjacent to the bushing a typical impact cavitation damage is produced as displayed in photo (Fig.10). Main feature is that the damage is in the size of the feedhole diameter.

4 Summary

In the present work the comparison of a cavitation experiment of a real journal bearing with the state of the art 2D-simulation and a full 3D-CFD simulation was presented. The calculations are done in respect to localize critical cavitation areas. Overall, the two-dimensional approach gives wrong information in 2 critical regions. Therefore, a three-dimensional approach performed to carry out the behavior of the cavitation phenomena. In the first step, the numerical results were

evaluated with experimental data, which were obtained quantitatively by velocity measurements using LDV-technique to compare velocity profiles with a high spatial resolution. The two-phase model validated on experiment from literature, which is similar to journal bearing system.
The advantage of the three-dimensional simulation is shown by obtaining the vapour distribution in the gap between the shaft and the bushing of the journal bearing. The paper illustrates the needs of three-dimensional approach for capturing the onset of cavitation, the vapour production, in real journal bearing.
Future activities include the extension of the CFD calculation towards unsteady movement of the shaft due the unsteady loads in internal combustion engines.

5 Nomenclature

B	breadth of the bearing
d_B	diameter of feedhole
e	eccentricity
h	local gap width
H_0	bearing clearance
Q_0	main volume flow
Q_{in}	volume flow of incoming oil
p	pressure
R_1	radius of the inner cylinder
R_2	radius of the outer cylinder
Re	Reynolds number
U_1	circumferential velocity of the inner cylinder
$\boldsymbol{u}$	flow velocity vector
α	vapour fraction
φ	angle
ν	kinematic viscosity
ρ	density
ε	relative eccentricity
φ_{AB}	angle of the outflow feedhole position
ψ	normalized clearance
ω	angular speed of the inner cylinder

6 References

[1] P.Stücke, M.Nobis, M.Schmidt, 2009: „3D-Flow Structures in Journal Bearings“ SAE Powertrains Fuels and Lubricants, SAE International, 2009

[2] M. Schmidt, P. Stücke, M. Nobis 2011: „ Numerical meshing issue for three-dimensional flow simulation in journal bearings “ 3rd Micro and Nanoflow Conference, Thessaloniki Greece

[3] Sauer J., 2000; „Instationär kavitierende Strömungen - Ein neues Modell basierend auf Front Capturing (VoF) und Blasen-dynamik“, Dissertation, Universität Karlsruhe

[4] Wollfarth, M., 1995, „Experimentelle Untersuchungen der Kavitationserosion im Gleitlager“, Dissertation, Universität Karlsruhe

[5] Jakobsson, B., Floberg, L., 1957: „The finite journal bearing considering vaporization", Transactions of Chalmers University of Technology

[6] S.Cupillard, Glavatskih, S., Cervantes, M. 2008:„ Computational fluid dynamics analysis of a journal bearing with surface texturing “Proceedings of the Institution of Mechanical Engineers, Part J, Journal of Engineering Tribology

[7] FVV e.V, 2013: „3D-CFD-Simulation der Schmierspaltströmung in einem hydro-dynamisch geschmierten, instationär belasteten Radialgleitlager “, Schlussbericht, Aif 16805BG .